

Role of Calcium in Metalloenzymes: Effects of Calcium Removal on the Axial Ligation Geometry and Magnetic Properties of the Catalytic Diheme Center in MauG

Yan Chen,[†] Sunil G. Naik,[†] J. Krzystek,[‡] Sooim Shin,^{||} William H. Nelson,[§] Shenghui Xue,[‡] Jenny J. Yang,[†] Victor L. Davidson,^{||} and Aimin Liu^{*,†}

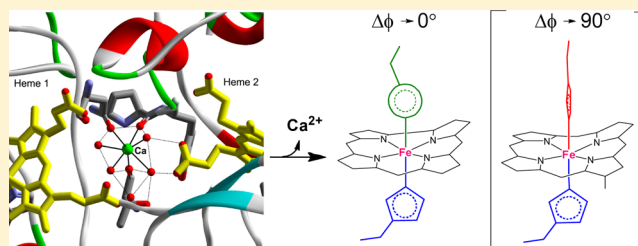
[†]Department of Chemistry, [‡]Department of Biology, and [§]Department of Physics and Astronomy, Molecular Basis of Disease Program, Georgia State University, P.O. Box 4098, Atlanta, Georgia 30303, United States

^{||}Burnett School of Biomedical Sciences, College of Medicine, University of Central Florida, Orlando, Florida 32827, United States

[‡]National High Magnetic Field Laboratory, Florida State University, Tallahassee, Florida 32310, United States

S Supporting Information

ABSTRACT: MauG is a diheme enzyme possessing a five-coordinate high-spin heme with an axial His ligand and a six-coordinate low-spin heme with His-Tyr axial ligation. A Ca^{2+} ion is linked to the two hemes via hydrogen bond networks, and the enzyme activity depends on its presence. Removal of Ca^{2+} altered the electron paramagnetic resonance (EPR) signals of each ferric heme such that the intensity of the high-spin heme was decreased and the low-spin heme was significantly broadened. Addition of Ca^{2+} back to the sample restored the original EPR signals and enzyme activity. The molecular basis for this Ca^{2+} -dependent behavior was studied by magnetic resonance and Mössbauer spectroscopy. The results show that in the Ca^{2+} -depleted MauG the high-spin heme was converted to a low-spin heme and the original low-spin heme exhibited a change in the relative orientations of its two axial ligands. The properties of these two hemes are each different than those of the heme in native MauG and are now similar to each other. The EPR spectrum of Ca^{2+} -free MauG appears to describe one set of low-spin ferric heme signals with a large g_{max} and anisotropy and a greatly altered spin relaxation property. Both EPR and Mössbauer spectroscopic results show that the two hemes are present as unusual highly rhombic low-spin hemes in Ca^{2+} -depleted MauG, with a smaller orientation angle between the two axial ligand planes. These findings provide insight into the correlation of enzyme activity with the orientation of axial heme ligands and describe a role for the calcium ion in maintaining this structural orientation that is required for activity.



It is widely recognized that Ca^{2+} ions are central to complex intracellular messenger systems that mediate a broad range of biological processes: muscle contraction, secretion, glycolysis and gluconeogenesis, ion transport, cell division, and cell growth.¹ For instance, there are a number of proteins that belong to the calmodulin superfamily that are known to be intracellular Ca^{2+} -triggered proteins.^{2,3} Calcium ion is found to regulate enzymes such as protein kinase C,⁴ phospholipase A_2 ,⁵ α -amylase,⁶ and nucleases by binding at or near the active site to control their catalytic functions.⁷ Most endothelial and neuronal nitric oxide synthases are Ca^{2+} -dependent with respect to the production of nitric oxide.⁸ Ca^{2+} binding in the proximity of catalytic hemes is also reported in *b*-type heme peroxidases and *c*-type diheme peroxidases. The function of Ca^{2+} in bacterial diheme protein cytochrome *c* peroxidase (CcP) has been postulated as maintenance of the heme conformation, rearrangement of the internal hydrogen bond network, and modulation of the electron transfer rates between the two domains of the protein,⁹ and it also affects the electrochemical behavior of the two hemes.¹⁰ It is important to understand the

molecular mechanism by which calcium is used in the regulation of metalloenzymes.

MauG is a *c*-type diheme enzyme that is homologous in sequence and structure to bacterial diheme CcP enzymes.^{11,12} However, MauG does not function as a cytochrome *c* peroxidase; instead, MauG uses H_2O_2 to catalyze posttranslational modifications of its protein substrate.¹³ The chemical reaction mediated by MauG is an unusual six-electron oxidation required for conversion of a precursor of methylamine dehydrogenase (preMADH) to its catalytically active form that contains a protein-derived tryptophan tryptophylquinone (TTQ) cofactor.^{14,15} The crystal structure of the MauG–preMADH complex reveals the presence of a Ca^{2+} ion in the proximity of the two hemes (Figure 1).¹² The orientation of the Ca^{2+} and two hemes in MauG is similar to that in the CcPs. Ca^{2+} binding is associated with conversion of the CcP enzyme from an inactive diferric form to an active mixed-valence form.

Received: October 15, 2011

Revised: February 7, 2012

Published: February 8, 2012

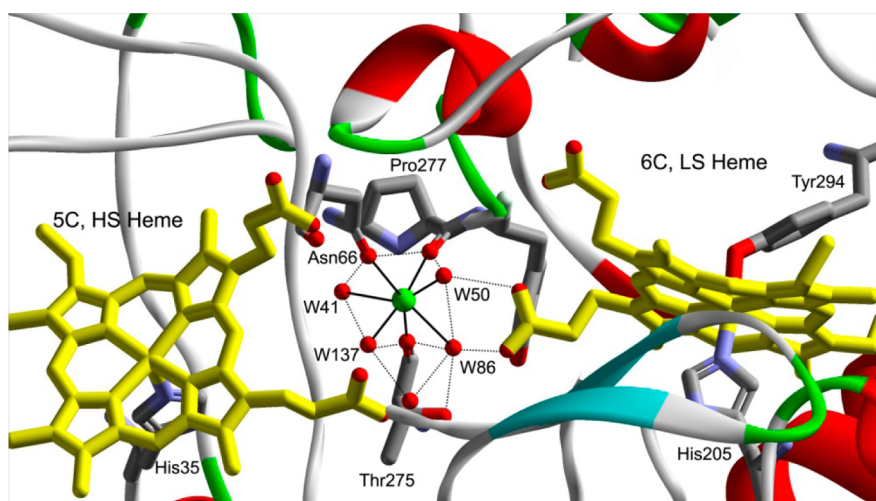


Figure 1. Structure of the calcium binding site, five-coordinate high-spin (5C, HS), and six-coordinate low-spin (6C, LS) hemes in MauG (Protein Data Bank entry 3L4M).¹² The H-bond network around the Ca^{2+} ion is shown with dotted lines. For the sake of clarity, Trp93 and loops in front of the Ca^{2+} ion and hemes were omitted. W designates water molecules.

In contrast, the Ca^{2+} of MauG does not readily dissociate or appear to play a regulatory role in the catalytic cycle. It was previously shown that MauG exhibited altered absorption and resonance Raman spectra and was no longer able to catalyze TTQ biosynthesis after extensive treatment with Ca^{2+} ion chelators.¹⁶ After addition of Ca^{2+} to the Ca^{2+} -depleted MauG, full TTQ biosynthesis activity and reactivity toward H_2O_2 were restored, and the spectral properties returned to those of native MauG. The circular dichroism spectra of native and Ca^{2+} -depleted MauG were essentially the same, consistent with Ca^{2+} -induced conformational changes involving domain or loop movements rather than general unfolding or alteration of secondary structure.¹⁶

The crystal structure of the MauG–preMADH protein complex reveals that the two ferric ions of the hemes are 21 Å apart. The five-coordinate high-spin ferric heme, which reacts with H_2O_2 to generate a catalytic bis-Fe(IV) intermediate,¹⁷ is positioned more than 40 Å from the two substrate tryptophan residues of preMADH. Residue Trp93 and a Ca^{2+} ion are both positioned between the two hemes.¹² The Ca^{2+} ion in MauG, ~12 Å from each Fe ion, is coordinated by seven oxygen atoms from the carboxyl oxygen of Asn66, the amide carboxyl oxygens of Pro277 and Thr275, and four well-ordered structural water molecules (Figure 1). Propionate substituents of both hemes of MauG are linked to the Ca^{2+} ion via hydrogen-bonded water molecules. Previous results indicate that the presence of Ca^{2+} is critical in maintaining an appropriate structural environment for the hemes, which allows MauG to generate the unprecedented bis-Fe(IV) intermediate and catalyze a complex six-electron oxidation of a protein substrate.^{16,17} However, how the Ca^{2+} ion helps to organize the catalytic diiron center and maintain the functionally active state remains unknown. Thus far, it has not been possible to crystallize the inactive Ca^{2+} -depleted MauG. In this study X-band and high-field EPR (HF-EPR) spectroscopy, proton relaxometry, and Mössbauer spectroscopy are used to characterize the structure and unusual magnetic properties of the hemes in Ca^{2+} -depleted MauG. The results reveal a significant, reversible, Ca^{2+} -dependent change in the nature and orientation of the axial ligands of the two hemes, which profoundly influences the axial ligation geometry and magnetic properties of both hemes. This is a previously

unreported role for calcium ion in maintaining the proper heme orientations that are required for activity.

EXPERIMENTAL PROCEDURES

Protein Preparation. The preparation of MauG has been described previously.¹¹ The concentration of MauG was calculated using the extinction coefficient of the Soret band of the heme groups ($\epsilon_{406} = 309000 \text{ M}^{-1} \text{ cm}^{-1}$).¹⁸ Ca^{2+} -depleted MauG was prepared by incubating 10 mM EDTA or EGTA with native MauG at 4 °C overnight and then desalting the protein with a prepacked G-25 column from GE Healthcare in 50 mM potassium phosphate buffer (pH 7.5). Ca^{2+} -depleted MauG was reconstituted with Ca^{2+} by changing the potassium phosphate buffer of Ca^{2+} -depleted MauG into 50 mM Tris buffer (pH 7.5) followed by overnight incubation with 10 mM calcium chloride at 4 °C. Free metal ions were removed by passing the samples through a 5 mL HiTrap Desalting Column (GE Healthcare).

X-Band EPR Spectroscopy. The continuous-wave X-band EPR spectra were recorded at liquid-helium temperatures on a Bruker ER200D spectrometer at a 100 kHz modulation frequency using a 4116DM resonator. The sample temperature was maintained with an ITC503S controller, an ESR910 cryostat, and a LLT650/13 liquid helium transfer tube (Oxford Instruments, Concord, MA). EPR simulations were performed using the EPR simulation program SPIN.¹⁹ The EPR relaxation behavior of the ferric hemes was characterized by the parameters of the saturation curves in terms of the microwave power at half-saturation ($P_{1/2}$) and b , which describes the contribution of inhomogeneous broadening according to eq 1:^{20–22}

$$I \propto \frac{\sqrt{P}}{(1 + P/P_{1/2})^{b/2}} \quad (1)$$

where I is the EPR derivative signal amplitude (peak-to-peak height) and P is the microwave power. It is known that dipole coupling can lead to significant errors in the determination of spin relaxation times.²² However, the two heme Fe ions in MauG are 21 Å apart. The dipolar–dipolar interactions are not

detectable to any significant degree. Thus, eq 1 is applicable to MauG.

High-Field EPR. HFEPR spectra were recorded at the EMR Facility at the National High Magnetic Field Laboratory (NHMFL).²³ A Virginia Diodes (Charlottesville, VA) source operating at a base frequency of 12–14 GHz and multiplied by a cascade of multipliers was used in conjunction with a 15/17 T superconducting magnet. Detection was achieved with an InSb hot-electron bolometer (QMC Ltd., Cardiff, U.K.). The magnetic field was modulated at 50 kHz. A Stanford Research Systems SR830 lock-in amplifier converted the modulated signal to DC voltage. The low temperature was achieved with an Oxford Instruments (Oxford, U.K.) continuous flow cryostat and a temperature controller from the same source.

Mössbauer Spectroscopy. ⁵⁷Fe-enriched native MauG was prepared via a previously described procedure¹⁷ with minor modifications. Briefly, LB medium was passed through Chelex-100 resin. The ⁵⁷Fe stock solution was prepared by dissolving ⁵⁷Fe metal powder (95.4% ⁵⁷Fe enrichment, Science Engineering & Education Co.) in 2.5 M H₂SO₄ under anaerobic conditions. The iron and acid mixture was incubated at 60 °C while being stirred in an anaerobic chamber until the ⁵⁷Fe metal was completely dissolved in the acid. The ⁵⁷Fe solution (0.72 M) was added to the Chelex-100-treated LB medium to a final concentration for 80 μM for preparation of the cell culture. The ⁵⁷Fe-enriched native MauG and ⁵⁷Fe-enriched Ca²⁺-depleted MauG (1 mM, 400 μL, isolated from a 60 L cell culture for each sample) were transferred into delrin cups and subjected to Mössbauer analyses while frozen. Mössbauer spectra were recorded in a weak-field spectrometer equipped with a Janis 8DT variable-temperature cryostat at Emory University (Atlanta, GA). The zero velocity of the spectra refers to the centroid of a room-temperature spectrum of a metallic iron foil.

Proton NMR Relaxometry. *T*₁ and *T*₂ of the native MauG and Ca²⁺-depleted MauG were measured on a Bruker Minispec mq60 NMR analyzer at 4 °C. Native and Ca²⁺-depleted MauG samples (at 150 μM) were placed in a quartz tube, and their relaxation times were measured. *r*₁ and *r*₂ were calculated with the following equations:

$$r_1 = \left(\frac{1}{T_1} - \frac{1}{T_{1\text{buffer}}} \right) / [\text{heme}] \quad (2)$$

$$r_2 = \left(\frac{1}{T_2} - \frac{1}{T_{2\text{buffer}}} \right) / [\text{heme}] \quad (3)$$

RESULTS

X-band EPR Spectroscopy. The low-temperature X-band EPR spectrum of native MauG shows three ferric heme species (Figure 2A): (i) a high-spin (*S* = 5/2) heme with *g* values of 1.99 and a 5.57 that can be assigned to the five-coordinate (5C) His-ligated heme (designated HS heme hereafter), (ii) a low-spin (*S* = 1/2) heme with *g* values of 1.87, 2.19, and 2.54 that is assigned to the six-coordinate (6C) His-Tyr-ligated heme (designated LS heme hereafter), and (iii) a second broad and low-intensity low-spin (*S* = 1/2) heme observed at *g* values of 1.52, 2.32, and 2.89, which is derived from the high-spin heme upon freezing.¹¹ The HS and LS hemes have been previously shown to exhibit distinct relaxation properties, with the LS heme more easily saturated by the applied microwave power. The EPR spectrum of native MauG, shown in Figure 2A, was obtained at 10 K with a microwave power of 1 mW. This was

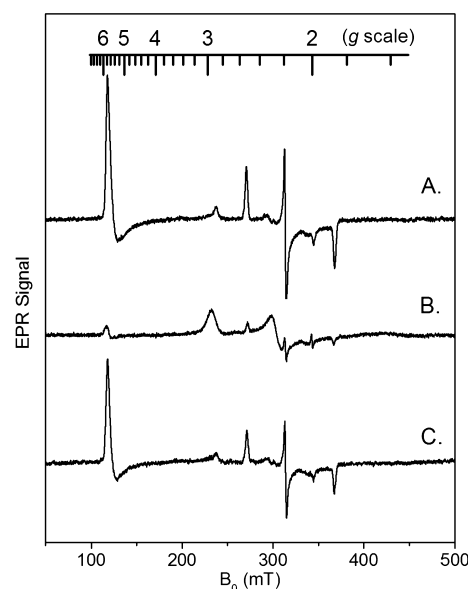


Figure 2. X-Band EPR spectra of MauG (A), Ca²⁺-depleted MauG (B), and the Ca²⁺-depleted MauG that was reconstituted with Ca²⁺ (C). EPR conditions: temperature of 10 K, microwave frequency of 9.6 GHz, microwave power of 1 mW, and scan time of 160 s. The *g* scale is shown at the top.

found to be the optimal condition for observing both the HS and LS hemes in MauG. Upon relatively extensive treatment with EDTA or EGTA [while maintaining protein stability (see Experimental Procedures)], MauG's catalytic activity is nearly lost, and its absorption and resonance Raman spectra are altered.¹⁶ In the EPR spectrum of the Ca²⁺-depleted MauG (Figure 2B), most of the original HS and LS ferric heme EPR signals disappear. The remaining signals have <10% of their original intensity and likely arise from a subpopulation of residual native MauG from which Ca²⁺ was not completely removed after extensive treatment with EDTA or EGTA. A single new low-spin heme EPR signal (*g* values of 1.50, 2.27, and 2.97) appears in the Ca²⁺-depleted MauG spectrum, which is broader and has a much lower intensity than the original LS ferric heme EPR signal (designated as LS* heme hereafter). Because of its low amplitude, this new LS* EPR signal can be easily underestimated, leading to a proposition that the diferric hemes changed from the EPR-active states to what appears to be an EPR-inactive state in the X-band EPR spectrum (Figure 2). When the Ca²⁺-depleted MauG sample was reconstituted with Ca²⁺, the EPR signals returned to those of the original native MauG (Figure 2C). Thus, this apparent loss of EPR signal intensities from the two ferric hemes, caused by depletion of Ca²⁺, is a reversible process that affects the catalytic activity of MauG.

While it is apparent the EPR signal intensity of the HS ferric heme decreased in the Ca²⁺-depleted MauG sample, the LS heme appeared to become noticeably broadened. The *g* anisotropy (*g*_x − *g*_z) of the LS heme is 0.67. This value is 1.37 for LS* after depletion of Ca²⁺. The broad LS* species spans more than nearly 300 mT in the EPR spectrum. Unlike the HS heme EPR signal, the LS and LS* species cannot be directly quantitated from their EPR signals because of overlapping resonances in the spectrum. To circumvent the difficulty in quantitation, we performed EPR simulations. We were able to simulate both the LS and LS* species. The theoretically reconstructed EPR spectrum in the *g* = 2 region is shown in

Figure 3. The results show that ~10% of the EPR signals were contributed from the original LS ferric heme.

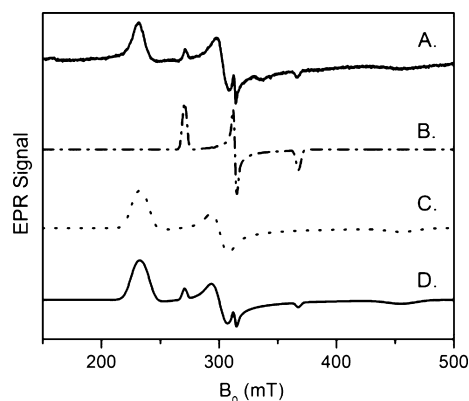


Figure 3. EPR spectrum and simulation of low-spin ferric hemes in the Ca^{2+} -depleted MauG. (A) Experimental spectrum obtained at 10 K with a microwave power of 1 mW, (B) spectrum of the simulated LS species, (C) spectrum of the simulated LS^* species, and (D) simulated spectrum with 0.1 LS and 0.9 LS^* .

Because the c -type hemes of MauG are covalently bound, it is unlikely that this apparent loss of the EPR signal amplitude upon depletion of Ca^{2+} is due to the loss of heme. After the metal chelator treatment, the enzyme was desalted through a column. With addition of Ca^{2+} , but not iron ion, the EPR signals re-emerged. It is also unlikely that the ferric hemes are converted to EPR-silent redox states, such as Fe(II) or Fe(IV) , by treatment with the metal chelators. This leaves two other plausible possibilities that may lead to the significant reduction of the amplitude of the ferric heme EPR signals. One is that the two ferric ions ($S = 1/2$ and $S = 5/2$, respectively) become spin-coupled to produce a non-Kramers integer ground spin state ($S = 2$ or 3), which typically cannot be accessed by conventional X-band EPR because of a large zero-field splitting. A second possibility is that the electron spin resonance and EPR relaxation properties of the ferric hemes have changed considerably such that their EPR signals are broadened, resulting in substantial reductions in the signal amplitudes that are much smaller than those in the native MauG at the given microwave power. To test these possibilities and to determine the structural basis for the observed changes in the electronic properties in the Ca^{2+} -depleted MauG, we used Mössbauer and multifrequency EPR spectroscopy as well as proton relaxivity measurements to probe the status of the heme iron ions in the native and Ca^{2+} -depleted MauG samples.

High-Field EPR Spectroscopy. To more precisely characterize the difference in the properties of ferric LS heme of native MauG and LS^* heme of Ca^{2+} -depleted MauG, we recorded their EPR spectra in high field where the differences become more apparent and g anisotropy typically becomes better resolved (Figure 4). These spectra are dominated by fast-passage effects, resulting in their absorptive shape, rather than the standard first-derivative shape. The 104 GHz spectrum of the native form of MauG was simulated as a superposition of two low-spin ferric ions characterized by g matrices almost identical to those determined from X-band measurements. The major species is the original LS ferric heme with g values of 1.87, 2.19, and 2.54 with a linewidth of ~75 G. The other species is the low-spin ferric heme derived from the high-spin heme site upon freezing with g values of 1.52, 2.32, and 2.89

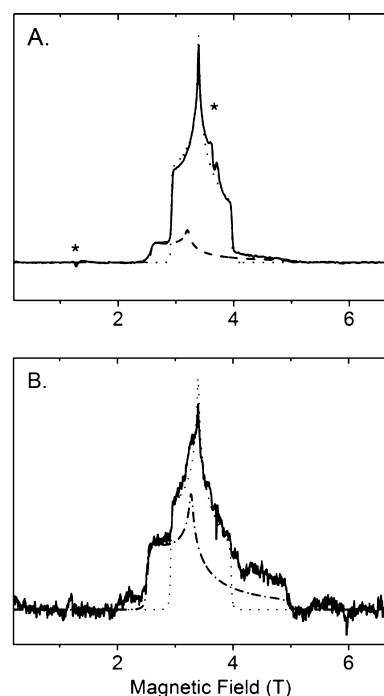


Figure 4. High-field and high-frequency (104 GHz) EPR spectra of native (A) and Ca^{2+} -depleted MauG (B) at 5 K with simulations. The HS heme is denoted with asterisks. The experimental data are shown as solid lines. The dotted line is the simulation of the LS heme in native MauG with g values of 2.545, 2.19, and 1.873; the dashed line (g values of 2.89, 2.32, and 1.52) in panel A presents the LS heme in native MauG derived from the high-spin heme upon freezing; The dashed-dotted line in panel B presents the newly formed LS^* heme in the Ca^{2+} -depleted MauG with g values of 2.97, 2.27, and 1.50.

and a larger anisotropic line width of 200–400 G. The HS heme is also visible with low intensity in the HFEPR spectrum because of the difference in relaxation properties. The HFEPR spectrum of Ca^{2+} -depleted MauG was simulated as a superposition of two low-spin ferric ions. One is attributed to the LS heme of residual native MauG. Given the relatively high affinity of MauG for Ca^{2+} , it was difficult to completely deplete Ca^{2+} , and this prevented it from being scavenged by the apo form from trace amounts of Ca^{2+} in the buffer. The other species is that of the LS^* heme that is characterized by g values of 1.50, 2.27, and 2.97 and by a large anisotropic line width of 200–400 G. As this signal accounts for nearly all the ferric heme present, it represents two low-spin heme centers with similar magnetic properties that were derived from the original HS and LS hemes.

Electron Spin Relaxation Properties. The low EPR signal amplitude of the LS^* relative to those of the heme signals in native MauG suggests that the conversion to LS^* may have affected the spin relaxation and power saturation behavior of the hemes. The HS and LS hemes of native MauG exhibit different half-power saturation values ($P_{1/2}$). We found that a microwave power of 1 mW was the optimal power for obtaining a spectrum that clearly shows the spectra of the two ferric hemes of native MauG at 10 K. At higher power values, the LS ferric heme EPR signal became severely saturated, while at lower power values, the intensity of the HS ferric EPR signal was very weak. However, the Ca^{2+} -depleted MauG appeared to be EPR-silent when a microwave power of 1 mW was used. Figure 5 shows EPR spectra for native and Ca^{2+} -depleted

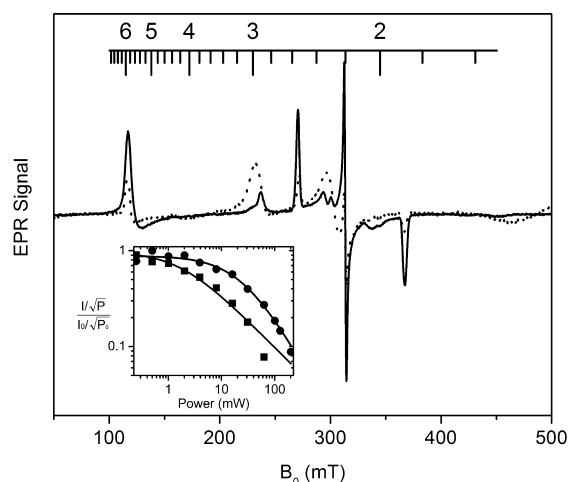


Figure 5. X-Band EPR spectra of native (···) and Ca^{2+} -depleted MauG (—) taken at 10 K. These spectra were taken with identical instrument parameters with the exception that the former was obtained with a microwave power of 1 mW and the latter with a microwave power of 12.7 mW. The inset is a plot of the 10 K power saturation profiles of the major low-spin ferric heme EPR signal in native (●) and Ca^{2+} -depleted MauG (■).

MauG where each was recorded using the most appropriate microwave power for observing multiple HS and LS species. The EPR signal intensity of LS* heme of Ca^{2+} -depleted MauG shown in Figure 5 that was taken with a >1 order of magnitude higher microwave power (12.7 mW) is now comparable to ferric heme EPR intensity of native MauG at the same protein concentration recorded with a 1 mW power and with otherwise the same temperature and instrument conditions. The total spins of LS* obtained at 12.7 mW account for nearly 90% of the total ferric ion of the two heme sites when compared to that in native MauG after integration of all EPR signals. The inset of Figure 5 shows the power saturation behavior of the new LS* species compared to that of the major LS ferric heme in native MauG. While the LS heme EPR signal becomes readily saturated when the microwave power approaches the milliwatt range, the power saturation profile of LS* is completely distinct and presents a $P_{1/2}$ value of 22.8 mW at 10 K. In contrast, the $P_{1/2}$ value of the LS species was 0.6 mW. The b values of LS and LS* were 0.96 and 1.3, respectively. These values suggest an inhomogeneous broadening of the EPR signals. The relatively poor fitting of the power saturation profile was caused by the fact that the full saturation was not reached by the instrumentation used. The presumed weak dipolar couplings between the two Fe ions may also contribute to the spin relation and can lead to errors in data analysis.²² This result indicates that the electron spin relaxations of the two hemes in the Ca^{2+} -depleted MauG are much faster than in the native MauG.

Mössbauer Spectroscopy. Figure 6 (top panel) displays the Mössbauer spectra of the ^{57}Fe -enriched MauG and Ca^{2+} -depleted MauG recorded at 180 K. Only quadrupole doublets are observed in these spectra, which indicate that the electronic relaxation is faster than the nuclear precession at this temperature. On the basis of the EPR spectrum of native MauG, which shows the presence of three different heme species, the spectrum of native MauG (Figure 6) was accordingly least-squares fit with three quadrupole doublets. One of the doublets (top panel, A, red line) with a ΔE_Q of 2.0

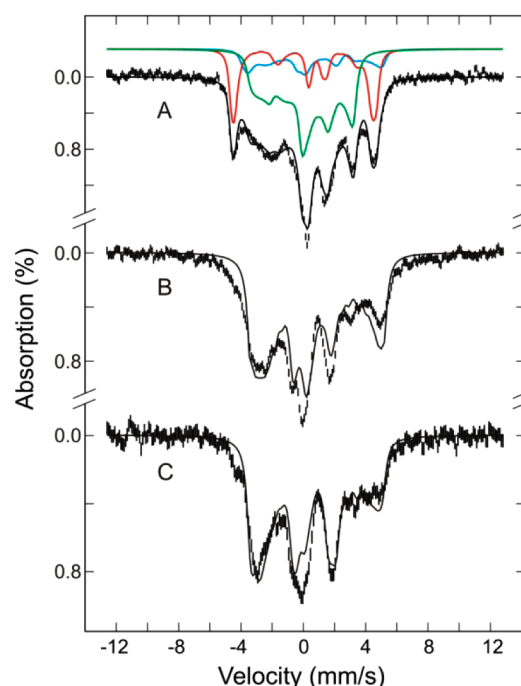
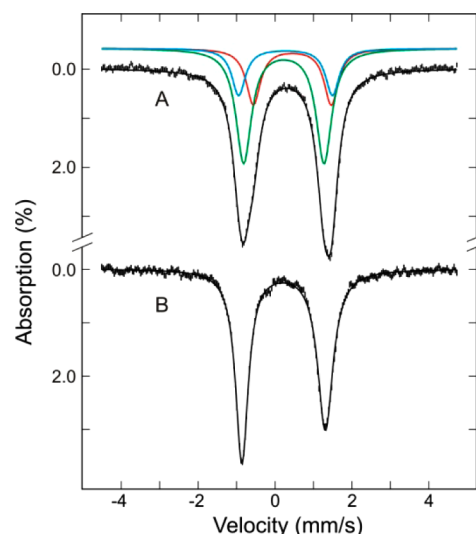


Figure 6. Mössbauer spectra (top panel) of the native ^{57}Fe -MauG (A) and Ca^{2+} -depleted MauG (B) samples recorded at 180 K with a field of 50 mT parallel to the γ -radiation. The solid black line overlaid on the experimental data (vertical bars) is the composite simulation. Spectrum A consists of high-spin (red line) and low-spin (green and cyan lines) ferric heme moieties. Spectrum B is simulated with only low-spin ferric heme. The parameters and the percent components of each Fe species are described in the text. Mössbauer spectra (bottom) of the ^{57}Fe -MauG (A) and Ca^{2+} -depleted MauG (B and C) samples recorded at 4.2 K in a field of 50 mT parallel (A and B) and perpendicular (C) to the γ radiation. The solid black line overlaid on the experimental spectrum (vertical bars) is the composite simulation. Spectrum A is simulated with a high-spin ferric heme (red line) and two low-spin ferric hemes (green and cyan lines). Spectra B and C are simulated with only low-spin ferric heme.

mm/s and a δ of 0.45 mm/s is characteristic of a HS ferric heme and accounts for 25% of the total Fe. The other two doublets are characteristic of low-spin ferric hemes with the following parameters: $\Delta E_Q = 2.44$ mm/s, and $\delta = 0.27$ mm/s (cyan line); $\Delta E_Q = 2.09$ mm/s, and $\delta = 0.23$ mm/s (green

line). Together both doublets account for 75% of the total Fe. The green doublet (55%) is assigned to the LS heme and the cyan doublet (20%) to the low-spin species derived from freezing of the HS heme. The 180 K Mössbauer spectrum of the Ca^{2+} -depleted MauG (B) is distinct from that of native MauG. The spectrum is sharper and shows apparently a smaller quadrupole splitting. In accord with the high-field EPR data of the Ca^{2+} -depleted MauG, which show that a majority (~90%) of the Fe is present in the LS^* state, the Mössbauer spectrum was least-squares fit with a single asymmetric quadrupole doublet. The parameters obtained ($\Delta E_Q = 2.17$ mm/s, and $\delta = 0.22$ mm/s) are characteristic of low-spin ferric heme, and the doublet is assigned to the LS^* heme. The minor spectral component (~10%) arising from the residual native MauG is unresolved and therefore is not considered in our analysis. Because of the minor contributions, its presence is not expected to have a significant effect on the determination of the parameters of LS^* heme.

To obtain a more detailed description of the magnetic properties of these hemes and to investigate directly whether the two LS^* heme moieties are spin-coupled in the Ca^{2+} -depleted MauG, we also recorded Mössbauer spectra at a low temperature (4.2 K) in the presence of a weak external magnetic field of 50 mT parallel or perpendicular to the γ -radiation (Figure 6, bottom panel). Magnetic hyperfine-split spectra are observed for both native MauG (A) and Ca^{2+} -depleted MauG (B and C), indicating unambiguously that, as in native MauG, the two heme groups in Ca^{2+} -depleted MauG are not spin-coupled. Consistent with analysis applied to the 180 K spectra, the 4.2 K native MauG spectrum (A) is also decomposed into three spectral components arising from the HS ferric species (25%, red line), the LS ferric species (55%, green line), and the low-spin species derived from freezing of the HS heme (20%, cyan line). The Mössbauer and spin Hamiltonian parameters of the HS and LS ferric species, listed in Table 1, are similar to those reported previously.¹⁷ The parameters for the low-spin species derived from freezing of the HS heme were obtained using the procedures described in the next paragraph and are also listed in Table 1.

The 4.2 K Ca^{2+} -depleted Mössbauer spectra (Figure 6, bottom panel, B and C) were simulated with a single low-spin ferric species, presumably the LS^* species. To this end, we employed a crystal field theory^{24,25} that has been used successfully to analyze low-spin ferric heme Mössbauer spectra²⁶ to estimate the A tensor from the observed g values (2.97, 2.27, and 1.52). In general, the quadrupole splitting for low-spin ferric complexes is relatively insensitive to temperature. The ΔE_Q value, 2.17 mm/s, obtained at 180 K was therefore used for the simulation of the 4.2 K spectra. Consequently, the only parameter that is varied in our simulation is the asymmetric parameter, η , which was varied until the simulation yielded theoretical spectra comparable with the experimental spectra. The solid lines plotted (90% of the total Fe absorption) over the experimental spectra (B and C) are results of theoretical simulations of LS^* using the parameters listed in Table 1. Despite the fact that our analysis did not take into consideration the minor presence (10%) of the leftover native MauG in the Ca^{2+} -depleted sample, the agreement between the experimental spectra and the simulated spectra of the major component (LS^*) is reasonably good. In Table 1, the crystal field parameters, Δ/λ and V/Δ , for the low-spin heme derived from freezing of HS and for LS^* calculated from the crystal field theory²⁴ are listed, where Δ and V are the

Table 1. Mössbauer and Spin Hamiltonian Parameters of the High- and Low-Spin Ferric Hemes in Native and Ca^{2+} -Depleted MauG

	native MauG hemes			Ca^{2+} -depleted MauG heme
	HS	LS^a	LS^b	LS^*
D^c (cm^{-1})	10			
E/D^c	0			
Δ/λ^c			2.95	3.43
V/Δ^c			0.68	0.55
g_x	5.57	1.87	1.52	1.50
g_y	1.99	2.19	2.32	2.27
g_z	1.99	2.54	2.89	2.97
$A_x/g_n\beta_n$ (T)	-18.0	-35.0	-38.7	-32.0
$A_y/g_n\beta_n$ (T)	-18.0	9.30	22.6	15.0
$A_z/g_n\beta_n$ (T)	-18.0	29.4	50.6	50.0
ΔE_Q (mm/s)	2.0	2.09	2.44 ^d	2.17 ^d
δ (mm/s)	0.50	0.25	0.33	0.28
η^e	0.4	-3.0	-3.0	-2.0

^aThe His-Tyr heme. ^bLow-spin species derived from freezing of the HS heme. ^c Δ and V are the axial and rhombic crystal field parameters, respectively, and λ is the spin-orbit coupling constant. D is zero-field splitting. E/D is the rhombicity parameter. $A_n/g_n\beta_n$ is the saturation field. ^dValue at 180 K. ^e $\eta = (V_{xx} - V_{yy})/V_{zz}$, where V_{ii} values are the principle components of the electric field gradient tensor.

axial and rhombic crystal field parameters, respectively, and λ is the spin-orbit coupling constant.

Proton Relaxometry. Proton NMR relaxometry was used to examine the conformational change of the hemes upon depletion of calcium through the comparison of the relaxivity of native and Ca^{2+} -depleted MauG proteins (Figure S1 of the Supporting Information). The relaxivity information obtained by this technique is different from the spin relaxivity retrieved via EPR spectroscopy. The purpose of doing this set of experiments was to obtain the information of the inner water molecules instead of the relaxivity of the hemes. The r_1 and r_2 values were calculated from eqs 2 and 3 from the T_1 and T_2 values obtained from data fitting in Figure S1 of the Supporting Information. A decrease in the r_1 and r_2 values of Ca^{2+} -depleted MauG was observed. The r_1 value changed from 1.359 ± 0.013 to $0.458 \pm 0.002 \text{ mM}^{-1} \text{ s}^{-1}$, while the r_2 value changed from 3.915 ± 0.008 to $1.653 \pm 0.004 \text{ mM}^{-1} \text{ s}^{-1}$. The decrease in the r_1 and r_2 values suggests that the removal of calcium changed the relaxation properties of the heme centers. As discussed later, the number of water molecules in the heme sites may have been altered because of the departure of the Ca^{2+} ion.

DISCUSSION

The calcium binding site in MauG is decidedly unusual, because the ligands do not consist of negatively charged residues such as Asp or Glu as commonly seen in the well-characterized Ca^{2+} binding sites of other proteins, yet the calcium binding in MauG is relatively tight ($K_d = 5.3 \mu\text{M}$),¹⁶ suggesting that ligand charge is not the sole factor influencing binding affinity. When the Ca^{2+} ion is removed, the structural changes cause enzyme inactivation, implying notable alterations occurred at the heme centers. In this work, we conducted an extensive spectroscopic study comparing Ca^{2+} -depleted MauG and the native enzyme. One of the two key findings in this work is that the presence or absence of Ca^{2+} in MauG exerts a significant influence on the magnetic properties of its two heme centers and the relative

Table 2. Comparison of EPR and Mössbauer Parameters for the LS* Hemes of Ca²⁺-Depleted MauG with Those of HALS and HALS-like Ferric Heme Species

species	principal g factor (g_x, g_y, g_z)	Mössbauer parameters (mm/s)	
		ΔE_Q	δ
Ca ²⁺ -depleted MauG LS* hemes	2.97, 2.27, 1.52	2.17	0.28
His-Met ligated hemes			
<i>Pseudomonas denitrificans</i> CcP ⁴⁵	3.41 (g_{max})	2.01	0.24
cytochrome c_2 (<i>Rhodospirillum rubrum</i>) ⁴⁷	3.13, 2.11, 1.23	2.26	0.31
DsrMKJOP transmembrane complex cytochrome c (<i>Allochrodatum vinosum</i>) ⁴⁸	2.96, 2.26, 1.50	N/A ^a	N/A ^a
<i>Pseudomonas stutzeri</i> cytochrome cd_1 , heme c ⁴⁹	2.997, 2.275, 1.4	N/A ^a	N/A ^a
His-Tyr ligated hemes			
ascorbate peroxidase S160Y mutant ⁵⁰	2.94, 2.27, 1.47	N/A ^a	N/A ^a
heme–HAS–ibuprofen complex ⁵¹	2.93, 2.27, 1.55	N/A ^a	N/A ^a
His-His ligated hemes			
<i>P. denitrificans</i> CcP ⁴⁵	2.89, 2.32, 1.51	2.52	0.31
<i>Pseudomonas aeruginosa</i> CcP ⁵²	2.96, 2.27, 1.49	N/A ^a	N/A ^a
cytochrome c_3 (<i>Desulfovibrio baculatus</i>) ⁵³	2.93, 2.26, 1.51	2.0	0.24
[(TMP)Fe(1-MeIm) ₂] ⁺ (models of bis-histidinecoordinated cytochromes) ^{54,55}	2.886, 2.325, 1.571	2.14	0.27
sulfite oxidase heme ⁵⁶	2.92, 2.25, 1.533	N/A ^a	N/A ^a

^aNot available.

orientation of the heme axial ligands. The second key finding of this work is that the hemes become HALS-like species when Ca²⁺ is absent. A discussion of our results follows.

HALS-like Hemes in Ca²⁺-Depleted MauG. Highly anisotropic low-spin (HALS) hemes have been known since the early work of Griffith,^{27,28} Blumberg and Peisach,^{29,30} Taylor,³¹ Bohan,³² Loew,³³ Walker,^{26,34–36} and many others (for reviews, see refs 35, 37, and 38). In the 1970s, a “truth diagram” with the ligand field parameters was defined by Blumberg and Peisach for the calculation of the g values. This diagram was experimentally examined on the ferric porphyrin complexes and proteins by Walker and many others (for reviews, see refs 35 and 37). The EPR studies have provided a detailed picture of g_{max} and g anisotropy in relation to the electronic structure of ferric porphyrins and hemes with highly axial or rhombic ligation of the heme axial ligands.

As described previously in this study, several independent spectroscopic techniques show that, upon depletion of the Ca²⁺ ion, the two heme sites undergo a dramatic structural change even though the overall protein secondary structure is relatively unaltered.¹⁶ In Ca²⁺-depleted MauG, more than 90% of the enzyme is in the Ca²⁺-free form. Other than the 10% of the leftover native MauG EPR signals, the remaining 90% of ferric hemes in Ca²⁺-depleted MauG are almost completely absent under the typical low-microwave power conditions (Figure 2). The signal intensities look comparable to those of native MauG only under higher-microwave power conditions (Figure 5). The two hemes in Ca²⁺-free MauG have become spectroscopically indistinguishable from each other. The results of the multi-frequency EPR and Mössbauer studies are consistent with significantly changed electromagnetic properties of the ferric hemes in Ca²⁺-depleted MauG. These spectroscopic data also point to a very large g_{max} (g_x in this case) value and g anisotropy ($g_x - g_z$) value in LS*, which suggest the formation of HALS-like heme species.

The hallmark of HALS is that its members present a very large g_{max} value (2.9–3.5) and g anisotropy ($g_{max} - g_{min}$). The two hemes in Ca²⁺-free MauG present as LS* species with similar EPR g values of 1.50, 2.27, and 2.97 and Mössbauer parameters ($\delta = 0.28$ mm/s, and $\Delta E_Q = 2.17$ mm/s). As this g_{max} value is at the low end or what some might consider below

the threshold for HALS, it is termed HALS-like. HALS species were divided into two subgroups by Walker.³⁵ Their spectroscopic properties were elaborated very recently in a review by Andersson and co-workers.³⁸ The highly axial systems present a perpendicular axial ligand plane (type I), and the highly rhombic strained configuration systems are type II. Upon removal of Ca²⁺, the structure of MauG changes such that the HS and LS hemes are each converted to HALS-like species with highly rhombic EPR signals. In the case of the high-spin ferric heme, the change in EPR properties is associated with the introduction of a new axial ligand that converts the heme to a low-spin form. In the case of the native low-spin ferric heme, the His and Tyr axial ligands are retained but must undergo a change in orientation and bond angles relative to the heme and each other.

While the Ca²⁺-depleted MauG has presumably two distinct sets of axial ligates in their HALS-like species, their EPR and Mössbauer parameters are nearly identical. This is not surprising because HALS and HALS-like, despite being ligated by different residues, are known to exhibit similar EPR and Mössbauer signals (Table 2). The EPR and Mössbauer parameters for Ca²⁺-free MauG resemble those exhibited by HALS-like with bis-His, His-Met, and His-Tyr ligation (Table 2). The correlation of plane orientation of the axial ligand groups with g values has been established for bis-His and His-Met HALS.³⁸ Such a structural correlation, however, has not been previously characterized for His-Tyr-ligated hemes because of the existence of very few examples of His-Tyr-ligated hemes.

Estimation of the Alteration of Heme Axial Ligand Orientation Angles. We have utilized the crystal field theory and the truth diagram to estimate the axial ligand plane angles. The nature of rhombic versus axial in the ligand plane orientation of HALS is characterized by the crystal field parameter V/Δ . The value of V/Δ can be directly obtained from simulation of the Mössbauer data (Table 1). It can also be calculated from precisely determined principal g values by HFEPR according to eqs 4 and 5. For a completely axial system (type I), i.e., the two axial protein ligands perpendicular with

each other in terms of their planes (Figure 7), $V/\Delta \rightarrow 0$. For a pure rhombic system, V/Δ is assumed to be close to 0.67.³⁸

$$\frac{V}{\xi} = \frac{g_x}{g_z + g_y} + \frac{g_y}{g_z - g_x} \quad (4)$$

$$\frac{\Delta}{\xi} = \frac{g_x}{g_z + g_y} + \frac{g_z}{g_y - g_x} - \frac{V}{2\xi} \quad (5)$$

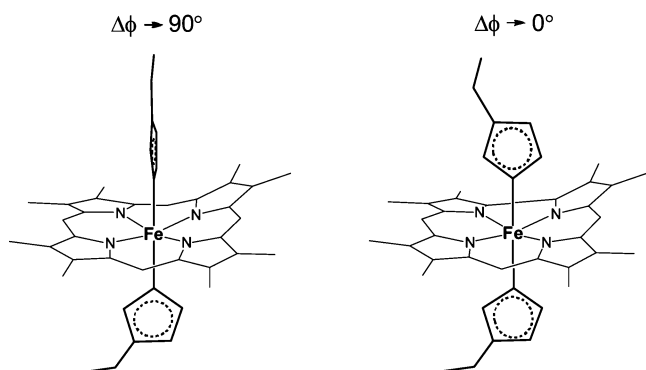


Figure 7. Cartoon illustration of the relative axial ligand plane angles in extreme HALS and HALS-like species using ferric hemes with two axial histidine ligands as an example.

We have attempted to interpret the EPR data by estimating the relative planar angles of the two aromatic rings of Tyr and His. The EPR and Mössbauer characterizations of those structurally defined systems of HALS, especially the single-crystal EPR studies, have suggested a pseudo-Jahn–Teller contribution to the crystal field, the magnitude of which depends on the orientation of the axial ligands.^{36,39,40} Quinn et al. characterized five synthesized bis-imidazole complexes by both X-ray crystallography and single-crystal EPR techniques.⁴⁰ The results suggest a linear correlation of the experimental values of V/Δ and $\Delta\phi$.⁴⁰ Versed in the knowledge of such a linear relationship and the two sets of the theoretical data, V/Δ (0 and 0.67) and the corresponding $\Delta\phi$ (90° and 0° , respectively), we formulated the following new equation for axial ligand plane angle estimations:

$$\Delta\phi = (0.67000 - V/\Delta)/0.00744 \quad (6)$$

When data points of ref 40 were fit, a similar equation was obtained (eq 7). While this equation is more pertinent to bis-imidazole complexes and the bis-His-ligated biological heme centers, it was of interest to apply it to the original five-coordinate HS data for Ca^{2+} -depleted MauG.

$$\Delta\phi = (0.70765 - V/\Delta)/0.00547 \quad (7)$$

The difference between eqs 6 and 7 is likely due to one of the axial ligands not being aligned in the straight axial position but instead bent at an angle even though the phenolate oxygen is always in the plane defined by the phenol ring of Tyr for the His-Tyr heme. Also, the crystal field parameters calculated from eqs 4 and 5 are slightly different from those obtained from Griffith's crystal field theory⁴¹ because eqs 4 and 5 approximate Griffith's theorem.⁴¹ From eqs 4 and 5, we calculated the value of V/Δ from HFEP for the new LS*. This number is 0.566 ($g_x = 1.50$, $g_y = 2.27$, and $g_z = 2.97$), which is approximately the same as that obtained from Mössbauer spectroscopy, 0.55

(Table 1). When the V/Δ value is plugged into eq 6, the calculated $\Delta\phi$ value is 14° (EPR) or 16° (Mössbauer spectroscopy), which is consistent with a more rhombic axial ligand plane. When eq 7 is used, the calculated $\Delta\phi$ value is 26° (from EPR data) or 29° (from Mössbauer data). Given these results, one may conservatively estimate that the angles of the axial heme ligand planes for the LS* species are between 14° and 29° (or $21 \pm 8^\circ$). This range is consistent with that of the so-called type II HALS (for a recent review, see ref 38) (Figure 7). The EPR and Mössbauer data led to very similar ligand orientation angle estimations (with a difference of only $2\text{--}3^\circ$). It should be kept in mind that the LS* species is actually two different hemes with indistinguishable properties. The estimation of the relative plane angle for LS* would not be applicable to the His-Tyr heme site, because the flexibility of the coordination of Tyr to the Fe ion can stray from the axial position and change the angle at the point of the phenolic oxygen. Although the actual $\Delta\phi$ value in the His-Tyr heme site cannot be estimated from the equations given above, the large g_{max} value and g anisotropy suggest a significant conformational change of $\Delta\phi$ in Ca^{2+} -free MauG, from 72° (discussed below) to a more rhombic ligand plane.

It should be noted that the $\Delta\phi$ value of the original LS in native MauG cannot be calculated from eqs 6 and 7, because LS in native MauG is not a HALS-like species. Fortunately, it can be obtained from the crystal structure of the MauG–preMADH complex. The Tyr ligand in the six-coordinate heme is not perpendicular to the heme plane.¹² It is inclined from the anticipated axial position. Using Discovery Studio Visualizer Client version 3.0 from Accelrys, the heme plane angle was measured to be 72° . Thus, the conversion of the LS heme to LS* heme is consistent with a dramatic change in the relative orientations of the His and Tyr heme ligands with respect to each other. It should be emphasized, however, that the angle calculations presented here are intended to be a qualitative argument rather than a quantitative one because of approximations described above.

Why Is Ca^{2+} -Depleted MauG Inactive? When the chemical nature of the heme centers is unraveled, we are no longer puzzled by the mystery of the enzyme inactivation in MauG associated with depletion of the Ca^{2+} ion. Although two hemes are present in MauG, only one of them reacts with an external oxidant. The originally five-coordinate (5C, His-ligated) HS heme site is known to be the reactive site with the oxidant, and the six-coordinate (6C, His-Tyr-ligated) LS heme shares electrons and charges with the 5C heme. The 5C ferric heme reacts with hydrogen peroxide and initially generates a ferryl and a cation radical. The radical immediately oxidizes the 6C heme and generates a bis-Fe(IV) heme.¹⁷ In the reduced state, the 5C ferrous heme reacts with CO, NO, and presumably O_2 while the His-Tyr-ligated heme is inaccessible to external small molecules.⁴² These conclusions were obtained in our previous biochemical and EPR study and recently confirmed by X-ray crystallography.⁴³ Upon removal of the Ca^{2+} ion, we found that the 5C HS heme is present as a 6C HALS-like species. In Ca^{2+} -depleted MauG, the H_2O_2 binding site is occupied by an amino acid residue or a solvent-derived molecule from the protein, so that the enzyme is not catalytically active.

At the originally five-coordinate (5C) heme site, the identity of the new axial sixth heme ligand that converts the HS heme to a LS* heme is not known. In *Pseudomonas nautica* CcP, the 5C heme picks up a distal His71 and generates a bis-His-ligated LS

heme. It is not clear if the structurally characterized *P. nautica* CcP bis-His-ligated LS heme is a HALS species, but the bis-His in *P. denitrificans* CcP is HALS-like (Table 2). The corresponding His71 is not found in the MauG sequence. Instead, a Met (residue 114 in MauG or 115 in some of the other family members) is conserved over the broader group of sequences, which may be an alternative distal heme ligand in Ca^{2+} -free MauG. Inspection of the crystal structure of native MauG for nearby residues reveals that Asp, Glu, and Met, but not His residues, could potentially provide a heme ligand. These residues are within 10 Å of the heme Fe ion in the distal pocket of the 5C HS heme. Barring a major structural rearrangement, it is not likely for His-His ligation to occur in the HALS-like species in MauG. Previous circular dichroism and resonance Raman studies, however, did not support a major structural rearrangement.¹⁶ Unfortunately, it is not yet possible to crystallize Ca^{2+} -depleted MauG. Identification of the added sixth ligand to the 5C HS heme upon removal of Ca^{2+} in MauG will be the subject of future study. On the basis of the available information, it seems most likely that a Met residue is repositioned and provides the distal axial ligand in the Ca^{2+} -free MauG.

Freezing Effect. As previously reported, when the native MauG is frozen, a fraction of the HS ferric heme is converted to low-spin.¹⁷ This is not a problem in this study because the 5C heme has already been converted to a 6C ferric heme species during the depletion of Ca^{2+} from MauG. However, such a cooling effect does cause complications when comparing the data of Ca^{2+} -depleted MauG with those obtained from native MauG. Approximately half of the originally 5C HS heme in native MauG (the control sample), or 25% of the total heme, becomes LS heme when the concentrated samples are frozen. Such a high-spin-to-low-spin transition upon cooling the enzyme has been found in other di-heme enzymes. For example, the HS heme in oxidized *P. denitrificans* CcP nearly completely converts to LS heme upon being frozen.^{44,45} *P. denitrificans* CcP and MauG are closely related periplasmic proteins. The two enzymes share a noticeable amino acid sequence similarity.¹⁵ The LS hemes generated by cooling in the two di-heme enzymes also show nearly identical spectroscopic properties.

The EPR and Mössbauer parameters for the artifactual LS species derived from the freezing effect in both native MauG and *P. denitrificans* CcP are very similar to those of the LS* species in Ca^{2+} -free MauG, although not identical. This suggests that structural changes at the originally HS site of native MauG occurring during freezing may be similar to those that occur during the removal of Ca^{2+} in solution. A water molecule is located approximately 3.7–3.8 Å from the HS heme in two copies of the native MauG crystal structure. A similar water molecule is present in the distal pocket of the 5C heme in bacterial di-heme CcP structures (Protein Data Bank entries 1RZ5 and 2VHD). The water molecule is likely the candidate to ligate to the 5C heme during the cooling process. An experimentally relevant piece of information is the proton relaxivity study that suggests that the removal of Ca^{2+} alters the inner phase water content of MauG. The decrease in the values of the relaxivity parameters observed in the proton relaxation experiments is consistent with three possibilities. First, the spin quantum number (*S*) directly contributes to the longitudinal (T_{1m}) and transverse (T_{2m}) relaxation times of bonded water according to the equations included in the Supporting Information. The EPR and Mössbauer data show that the

removal of calcium causes a spin state change of one of the hemes from $5/2$ to $1/2$. This should increase both T_{1m} and T_{2m} (eqs S1 and S2 of the Supporting Information), which is consistent with the observation of decreased r_1 and r_2 values of the heme (eqs S3 and S4 of the Supporting Information). Second, the relaxivity parameters of r_1 and r_2 are a function of *n*, i.e., the number of water ligands present in the first coordination shell. The observed decrease in both relaxivity parameter values may well indicate a decrease in the number of water molecules near iron ions upon the removal of calcium. Third, it is also possible but less likely that the removal of calcium results in the change in τ_c , the effective dipolar correlation time (eqs S1–S4 of the Supporting Information), as seen in the characterization of phenylalanine hydroxylase.⁴⁶

Role of Ca^{2+} Ion. We have learned from our previous study that the two heme centers in native MauG must efficiently share electrons so that the critical bis-Fe(IV) intermediate is formed when the five-coordinate heme reacts with H_2O_2 .^{17,42} In the absence of the Ca^{2+} ion, there is no evidence that the bis-Fe(IV) state of MauG could be formed in the absence of the Ca^{2+} ion, implying that the communication between the two iron ions is obstructed because of the departure of the Ca^{2+} ion. Thus, a role of Ca^{2+} in MauG is to maintain an environment that facilitates the electronic communication with the catalytic di-heme center. In other words, a proper conformation of the enzyme active site and its rigidity depend on the presence of Ca^{2+} ion. It seems only possible with the Ca^{2+} ion bound in the proximity of the two hemes that the Fe ions will efficiently share electrons during the catalytic cycle without spin coupling.

In most of the as-isolated bacterial di-heme CcPs, the H_2O_2 -binding heme is blocked by the presence of a distal His ligand, so the His-His-ligated heme is not reactive to external small oxidants. The reduction of the other His-Met heme generates a mixed-valence state that triggers a Ca^{2+} -dependent conformational change in which the distal His is replaced with water and hence becomes reactive toward H_2O_2 . The mixed-valent Fe(II)–Fe(III) state is stable in CcPs because the redox potentials of the two hemes are widely separated by several hundred millivolts. In contrast, the intrinsic redox potentials of the two hemes of MauG are similar, so the hemes are oxidized and reduced simultaneously with no formation of a mixed-valence state.⁴² This highlights the fact that in CcPs, Ca^{2+} plays an important role in the regulation of activity by interconverting the enzyme between an inactive diferric state and an active mixed valence state. This is not the role of Ca^{2+} in MauG, as it is active in the diferric state and does not exhibit a mixed valence state under any conditions. A regulatory role of Ca^{2+} in MauG cannot be ruled out because the changes in the spectroscopic properties and enzymatic activity caused by removal of Ca^{2+} are reversed by re-addition of Ca^{2+} . However, as a reductant is not required for Ca^{2+} binding, it seems unlikely that Ca^{2+} would dissociate in the absence of chelators in its physiological localization in the periplasm.

SUMMARY

Calcium plays a wide range of vital roles in proteins. The ability to catalyze TTQ biosynthesis and the magnetic properties of the two hemes of MauG are significantly altered by the removal of a relatively tightly bound Ca^{2+} from MauG. Interestingly, these changes are reversible with the re-addition of CaCl_2 . Both the five-coordinate high-spin heme and six-coordinate low-spin heme are converted to highly rhombic low-spin hemes with similar electronic properties in Ca^{2+} -depleted MauG. This is

caused by introduction of a sixth ligand into the high-spin heme and reorientation of the His and Tyr axial ligands of the low-spin heme. In the Ca^{2+} -free form, the two ferric hemes are present as HALS-like species with highly rhombic axial ligands. Mössbauer spectroscopic data rule out the possibility of a direct spin coupling between the two hemes. The relaxation properties of the hemes in Ca^{2+} -depleted MauG are changed with a much increased half-power saturation value. Depletion of Ca^{2+} also reduces both r_1 and r_2 relaxivity values, consistent with a loss of inner phase water molecules that may explain the effects of Ca^{2+} on both hemes because it is connected to each by structural water networks. Thus, we conclude that the tightly bound Ca^{2+} of MauG profoundly influences the axial ligation geometry and magnetic properties of the catalytic diheme center. It is quite remarkable that depletion of Ca^{2+} so dramatically alters the chemical and magnetic properties of both hemes of MauG and changes the axial ligand orientations and that this alteration is reversible. Overall, this work provides a new example of protein-bound HALS-like hemes and a novel mechanism by which Ca^{2+} influences the protein structure to support the catalytic activity of a metalloenzyme. Moreover, this work also provides an example of a spectroscopically characterized His-Tyr-ligated heme.

■ ASSOCIATED CONTENT

■ Supporting Information

Figures S1 and further details of the proton NMR relaxometry study. This material is available free of charge via the Internet at <http://pubs.acs.org>.

■ AUTHOR INFORMATION

Corresponding Author

*Department of Chemistry, Georgia State University, P.O. Box 4098, Atlanta, GA 30303. Telephone: (404) 413-5532. Fax: (404) 413-5505. E-mail: feradical@gsu.edu.

Funding

This work was supported by National Science Foundation Grant MCB-0843537 (A.L.), National Institutes of Health Grants GM041574 (V.L.D.) and GM081749 (J.J.Y.), Georgia State University predoctoral fellowships (Y.C. and S.X.), and the Georgia Cancer Coalition Distinguished Scientist Program (A.L.).

Notes

The authors declare no competing financial interest.

■ ACKNOWLEDGMENTS

We thank Dr. Boi Hanh (Vincent) Huynh of Emory University for access to Mössbauer spectroscopy and his invaluable guidance in data analyses. We acknowledge Dr. Andrew Ozarowski for his EPR simulation program SPIN. HFEPR studies were supported by the National High Magnetic Field Laboratory, which is funded by the National Science Foundation through Cooperative Agreement DMR 0654118, the State of Florida, and the U.S. Department of Energy.

■ DEDICATION

This paper is dedicated to the memory of co-author Professor William H. Nelson, who died of a heart attack on December 19, 2010.

■ ABBREVIATIONS

EPR, electron paramagnetic resonance; HFEPR, high-frequency/high-field EPR; CcP, cytochrome *c* peroxidase; 5C, five-coordinate; 6C, six-coordinate; HS, high-spin; LS, low-spin; LS*, low-spin ferric ion with large *g* anisotropy; HALS, highly anisotropic/highly axial low-spin; preMADH, precursor of methylamine dehydrogenase; TTQ, tryptophan tryptophylquinone.

■ REFERENCES

- (1) Forsen, S. K., Jr. (1994) Calcium in biological systems. In *Bioinorganic Chemistry* (Bertini, I., Gray, B., Lippard, S. J., and Valentine, J. S., Eds.) University Science Books, Mill Valley, CA.
- (2) Heizmann, C. W., and Braun, K. (1992) Changes in Ca^{2+} -binding proteins in human neurodegenerative disorders. *Trends Neurosci.* 15, 259–264.
- (3) Kretsinger, R. H. (1987) Calcium coordination and the calmodulin fold: Divergent versus convergent evolution. *Cold Spring Harbor Symp. Quant. Biol.* 52, 499–510.
- (4) Nishizuka, Y. (1983) Calcium, phospholipid turnover and transmembrane signalling. *Philos. Trans. R. Soc. London, Ser. B* 302, 101–112.
- (5) Dennis, E. A. (1997) The growing phospholipase A2 superfamily of signal transduction enzymes. *Trends Biochem. Sci.* 22, 1–2.
- (6) Obeta, J. A. N., Okungbowa, J., and Ezeogu, L. I. (2000) Malting of sorghum: Further studies on factors influencing α -amylase activity. *J. Inst. Brew.* 106, 295–304.
- (7) Nikonava, L. V., Nanazashvili, M. G., Krotova, K. E., Nazarova, L. F., Rabaya, N. A., Prusakova, O. V., and Beletskii, I. P. (1998) Comparative study of Ca/Mg-dependent nucleases of the mammalian thymus. *Izv. Akad. Nauk, Ser. Biol.* 2, 180–186.
- (8) Dennis, J. S. (1999) Mammalian nitric oxide synthases. *Biochim. Biophys. Acta* 1411, 217–230.
- (9) Dias, J. M., Alves, T., Bonifácio, C., Pereira, A. S., Trincão, J., Bourgeois, D., Moura, I., and Romão, M. J. (2004) Structural basis for the mechanism of Ca^{2+} activation of the di-heme cytochrome *c* peroxidase from *Pseudomonas nautica* 617. *Structure* 12, 961–973.
- (10) Lopes, H., and Pettigrew, G. W. (1998) Electrochemical study on cytochrome *c* peroxidase from *Paracoccus denitrificans*: A shifting pattern of structural and thermodynamic properties as the enzyme is activated. *J. Biol. Inorg. Chem.* 3, 632–642.
- (11) Wang, Y., Graichen, M. E., Liu, A., Pearson, A. R., Wilmot, C. M., and Davidson, V. L. (2003) MauG, a novel di-heme protein required for tryptophan tryptophylquinone biogenesis. *Biochemistry* 42, 7318–7325.
- (12) Jensen, L. M. R., Sanishvili, R., Davidson, V. L., and Wilmot, C. M. (2010) In crystallo posttranslational modification within a MauG/pre-methylamine dehydrogenase complex. *Science* 327, 1392–1394.
- (13) Li, X., Jones, L. H., Pearson, A. R., Wilmot, C. M., and Davidson, V. L. (2006) Mechanistic possibilities in MauG-dependent tryptophan tryptophylquinone biosynthesis. *Biochemistry* 45, 13276–13283.
- (14) Pearson, A. R., De la Mora-Rey, T., Graichen, M. E., Wang, Y., Jones, L. H., Marimanikkupam, S., Agger, S. A., Grimsrud, P. A., Davidson, V. L., and Wilmot, C. M. (2004) Further insights into quinone cofactor biogenesis: Probing the role of *mauG* in methylamine dehydrogenase tryptophan tryptophylquinone formation. *Biochemistry* 43, 5494–5502.
- (15) Davidson, V. L. (2001) Pyrroloquinoline quinone (PQQ) from methanol dehydrogenase and tryptophan tryptophylquinone (TTQ) from methylamine dehydrogenase. *Adv. Protein Chem.* 58, 95–140.
- (16) Shin, S., Feng, M., Chen, Y., Jensen, L. M., Tachikawa, H., Wilmot, C. M., Liu, A., and Davidson, V. L. (2011) The tightly bound calcium of MauG is required for tryptophan tryptophylquinone cofactor biosynthesis. *Biochemistry* 50, 144–150.
- (17) Li, X., Fu, R., Lee, S., Krebs, C., Davidson, V. L., and Liu, A. (2008) A catalytic di-heme bis-Fe(IV) intermediate, alternative to an Fe(IV)=O porphyrin radical. *Proc. Natl. Acad. Sci. U.S.A.* 105, 8597–8600.

- (18) Tarboush, N. A., Jensen, L. M. R., Feng, M., Tachikawa, H., Wilmot, C. M., and Davidson, V. L. (2010) Functional importance of tyrosine 294 and the catalytic selectivity for the bis-Fe(IV) state of MauG revealed by replacement of this axial heme ligand with histidine. *Biochemistry* 49, 9783–9791.
- (19) Ozarowski, A., Lee, H. M., and Balch, A. L. (2003) Crystal environments probed by EPR spectroscopy. Variations in the EPR spectra of Co(II)(octaethylporphyrin) doped in crystalline diamagnetic hosts and a reassessment of the electronic structure of four-coordinate cobalt(II). *J. Am. Chem. Soc.* 125, 12606–12614.
- (20) Portis, A. M. (1953) Electronic structure of F centers: Saturation of the electron spin resonance. *Phys. Rev.* 91, 1071–1078.
- (21) Castner, T. G. Jr. (1959) Saturation of the paramagnetic resonance of a V center. *Phys. Rev.* 115, 1506–1515.
- (22) Galli, C., Innes, J. B., Hirsh, D. J., and Brudvig, G. W. (1996) Effects of dipole-dipole interactions on microwave progressive power saturation of radicals in proteins. *J. Magn. Reson., Ser. B* 110, 284–287.
- (23) Hassan, A. K., Pardi, L. A., Krzystek, J., Sienkiewicz, A., Goy, P., Rohrer, M., and Brunel, L. C. (2000) Ultrawide band multifrequency high-field EMR technique: A methodology for increasing spectroscopic information. *J. Magn. Reson.* 142, 300–312.
- (24) Griffith, J. S. (1971) Theory of EPR in low-spin ferric hemoproteins. *Mol. Phys.* 21, 135–139.
- (25) Oosterhuis, W. T., and Lang, G. (1969) Mössbauer effect in potassium hexacyanoferrate(III). *Phys. Rev.* 178, 439–456.
- (26) Walker, F. A., Huynh, B. H., Scheidt, W. R., and Osvanth, S. R. (1986) Models of the cytochromes b. Effect of axial ligand plane orientation on the EPR and Mössbauer spectra of low-spin ferrihemes. *J. Am. Chem. Soc.* 108, 5288–5297.
- (27) Griffith, J. S. (1956) The magnetic properties of some hemoglobin complexes. *Proc. R. Soc. London, Ser. A* 235, 23–36.
- (28) Griffith, J. S. (1971) Theory of EPR in low-spin ferric hemoproteins. *Mol. Phys.* 21, 135–139.
- (29) Blumberg, W. E., and Peisach, J. (1971) in *Probes and Structure and Function of Macromolecules and Membranes* (Chance, B., Yonetani, T., and Mildvan, A. S., Eds.) Vol. 2, pp 215–229, Academic Press, San Diego.
- (30) Peisach, J., Blumberg, W. E., and Adler, A. (1973) Electron paramagnetic resonance studies of iron porphyrin and chlorin systems. *Ann. N.Y. Acad. Sci.* 206, 310–327.
- (31) Taylor, C. P. S. (1977) The EPR of low spin heme complexes. Relation of the t_{2g} hole model to the directional properties of the g tensor, and a new method for calculating the ligand field parameters. *Biochim. Biophys. Acta* 491, 137–149.
- (32) Bohan, T. L. (1977) Analysis of low-spin ESR spectra of ferric heme proteins: A reexamination. *J. Magn. Reson.* 26, 109–118.
- (33) Loew, G. H. (1970) Analysis of the electron spin resonance of low spin ferric heme compounds. *Biophys. J.* 10, 196–212.
- (34) Raitsimring, A. M., Borbat, P., Shokhireva, T. K., and Walker, F. A. (1996) Magnetic field (g-value) dependence of proton hyperfine couplings obtained from ESEEM measurements: Determination of the orientation of the magnetic axes of model heme complexes in glassy media. *J. Phys. Chem.* 100, 5235–5244.
- (35) Walker, F. A. (1999) Magnetic spectroscopic (EPR, ESEEM, Mössbauer, MCD and NMR) studies of low-spin ferriheme centers and their corresponding heme proteins. *Coord. Chem. Rev.* 185–186, 471–534.
- (36) Walker, F. A. (2006) The heme environment of mouse neuroglobin: Histidine imidazole plane orientations obtained from solution NMR and EPR spectroscopy as compared with X-ray crystallography. *J. Biol. Inorg. Chem.* 11, 391–397.
- (37) Walker, F. A. (2004) Models of the bis-histidine-ligated electron-transferring cytochromes. Comparative geometric and electronic structure of low-spin ferro- and ferrihemes. *Chem. Rev.* 104, 589–615.
- (38) Zoppellaro, G., Bren, K. L., Ensign, A. A., Harbitz, E., Kaur, R., Hersleth, H.-P., Ryde, U., Hederstedt, L., and Andersson, K. K. (2009) Studies of ferric heme proteins with highly anisotropic/highly axial low spin ($S = 1/2$) electron paramagnetic resonance signals with bis-histidine and histidine-methionine axial iron coordination. *Biopolymers* 91, 1064–1082.
- (39) Byrn, M. P., Katz, B. A., Keder, N. L., Levan, K. R., Magurany, C. J., Miller, K. M., Pritt, J. W., and Strouse, C. E. (1983) Low-spin ferric porphyrin complexes: Analysis of the electronic structure based on single-crystal electron spin resonance measurements. *J. Am. Chem. Soc.* 105, 4916–4922.
- (40) Quinn, R., Valentine, J. S., Byrn, M. P., and Strouse, C. E. (1987) Electronic structure of low-spin ferric porphyrins: A single-crystal EPR and structural investigation of the influence of axial ligand orientation and the effects of pseudo-Jahn-Teller distortion. *J. Am. Chem. Soc.* 109, 3301–3308.
- (41) Griffith, J. S. (1964) *The Theory of Transition-Metal Ions*, Cambridge University Press, Cambridge, U.K.
- (42) Fu, R., Liu, F., Davidson, V. L., and Liu, A. (2009) Heme iron nitrosyl complex of MauG reveals an efficient redox equilibrium between hemes with only one heme exclusively binding exogenous ligands. *Biochemistry* 48, 11603–11605.
- (43) Yuhl, E. T., Goblirsch, B. R., Davidson, V. L., and Wilmot, C. M. (2011) Crystal structures of CO and NO adducts of MauG in complex with pre-methylamine dehydrogenase: Implications for the mechanism of dioxygen activation. *Biochemistry* 50, 2931–2938.
- (44) Gilmour, R., Goodhew, C. F., Pettigrew, G. W., Prazeres, S., Moura, I., and Moura, J. J. G. (1993) Spectroscopic characterization of cytochrome c peroxidase from *Paracoccus denitrificans*. *Biochem. J.* 294, 745–752.
- (45) Prazeres, S., Moura, J. J. G., Moura, I., Gilmour, R., Goodhew, C. F., Pettigrew, G. W., Ravi, N., and Huynh, B. H. (1995) Mössbauer characterization of *Paracoccus denitrificans* cytochrome c peroxidase: Further evidence for redox and calcium binding-induced heme-heme interaction. *J. Biol. Chem.* 270, 24264–24269.
- (46) Olafsdottir, S., and Martínez, A. (1999) The accessibility of iron at the active site of recombinant human phenylalanine hydroxylase to water as studied by ¹H NMR paramagnetic relaxation. Effect of L-Phe and comparison with the rat enzyme. *J. Biol. Chem.* 274, 6280–6284.
- (47) Huynh, B. L., Emptage, M. H., and Munck, E. (1978) Mössbauer study of cytochrome c₂ from *Rhodospirillum rubrum*. Sign of the product $g_{xy}g_z$ of some low spin ferric heme proteins. *Biochim. Biophys. Acta* 534, 295–306.
- (48) Grein, F., Venceslau, S. S., Schneider, L., Hildebrandt, P., Todorovic, S., Pereira, I. A., and Dahl, C. (2010) DsrJ, an essential part of the DsrMKJOP transmembrane complex in the purple sulfur bacterium *Allochromatium vinosum*, is an unusual triheme cytochrome c. *Biochemistry* 49, 8290–8299.
- (49) Cheesman, M. R., Ferguson, S. J., Moir, J. W., Richardson, D. J., Zumft, W. G., and Thomson, A. J. (1997) Two enzymes with a common function but different heme ligands in the forms as isolated. Optical and magnetic properties of the heme groups in the oxidized forms of nitrite reductase, cytochrome cd₁, from *Pseudomonas stutzeri* and *Thiosphaera pantotropha*. *Biochemistry* 36, 16267–16276.
- (50) Pipirou, Z., Bottrill, A. R., Svistunenko, D. A., Efimov, I., Basran, J., Mistry, S. C., Cooper, C. E., and Raven, E. L. (2007) The reactivity of heme in biological systems: Autocatalytic formation of both tyrosine-heme and tryptophan-heme covalent links in a single protein architecture. *Biochemistry* 46, 13269–13278.
- (51) Nicoletti, F. P., Howes, B. D., Fittipaldi, M., Fanali, G., Fasano, M., Ascenzi, P., and Smulevich, G. (2008) Ibuprofen induces an allosteric conformational transition in the heme complex of human serum albumin with significant effects on heme ligation. *J. Am. Chem. Soc.* 130, 11677–11688.
- (52) Echalié, A., Brittain, T., Wright, J., Boycheva, S., Mortuza, G. B., Fulop, V., and Watmough, N. J. (2008) Redox-linked structural changes associated with the formation of a catalytically competent form of the diheme cytochrome c peroxidase from *Pseudomonas aeruginosa*. *Biochemistry* 47, 1947–1956.
- (53) Ravi, N., Moura, I., Costa, C., Teixeira, M., LeGall, J., Moura, J. J., and Huynh, B. H. (1992) Mössbauer characterization of the tetraheme cytochrome c₃ from *Desulfovibrio baculatus* (DSM 1743).

Spectral deconvolution of the heme components. *Eur. J. Biochem.* 204, 779–782.

(54) Safo, M. K., Gupta, G. P., Walker, F. A., and Scheidt, W. R. (1991) Models of the cytochromes *b*. Control of axial ligand orientation with a hindered porphyrin system. *J. Am. Chem. Soc.* 113, 5497.

(55) Teschner, T., Yatsunyk, L., Schunemann, V., Paulsen, H., Winkler, H., Hu, C. J., Scheidt, W. R., Walker, F. A., and Trautwein, A. X. (2006) Models of the membrane-bound cytochromes: Mössbauer spectra of crystalline low-spin ferriheme complexes having axial ligand plane dihedral angles ranging from 0° to 90°. *J. Am. Chem. Soc.* 128, 1379–1389.

(56) Kessler, D. L., and Rajagopalan, K. V. (1972) Purification and properties of sulfite oxidase from chicken liver. Presence of molybdenum in sulfite oxidase from diverse sources. *J. Biol. Chem.* 247, 6566–6573.